



Effect of Adding Biomass from Palm Kernel Shell on Phase Transformation and Microstructure during Carbothermic Reduction of Ilmenite

Cynta Immanuela Lamandasa¹, Agung Setiawan¹, Sri Harjanto^{1*}, M. Akbar Rhamdhani²

¹*Department of Metallurgical and Materials, Faculty of Engineering, Universitas Indonesia, Kampus UI Depok, Depok 16424, Indonesia*

²*Fluid and Process Dynamics (FPD) Research Group, Department of Mechanical and Product Design Engineering, Swinburne University of Technology, Melbourne, VIC 3122, Australia*

Abstract. This study investigated the effects of adding pulverized biomass from palm kernel shells as a reductant on phase transformation and microstructure during the carbothermic reduction of ilmenite. The ilmenite concentrate was reduced at a temperature range of 1000–1200°C for up to 3 h in an inert atmosphere. The amount of reducing agents used in this study varied between 6 and 10 wt.%. The reduced samples were studied using an X-ray diffractometer and optical microscope to analyze their phase transformations and microstructures. The results revealed that near-complete dissociation of ilmenite was attained when biomass was added up to 8 wt.%. Complete dissociation of ilmenite occurred, and Ti_3O_5 formed when ilmenite was reduced with 9 wt.% biomass at 1200°C for 2 h. At this point, the microstructural study showed that a significant amount of metallic iron, with an average metallic iron size of $241.5 \mu m^2$, had formed.

Keywords: Biomass; Carbothermic reduction; Ilmenite; Palm kernel shell

1. Introduction

The world's rutile reserves are low compared to ilmenite reserves ([U.S. Geological Survey, 2021](#)), and their amount is dwindling because rutile is still used in the titanium extraction process. An upgrading process is carried out to increase the titanium content by separating iron from titanium oxide in ilmenite and by increasing TiO_2 levels.

Currently, the upgrading process of ilmenite is carried out using the Becher, Murso, Laporte, Benelite, Austpac, Dunn, Kataoka, Altair, and BHP Billiton processes ([Nguyen and Lee, 2019](#)). However, the Becher, Murso, and Laporte processes require high energy consumption that yields high CO_2 emissions and are less effective due to the need to conduct an acid leaching process after pyrolysis. In addition, in the Benelite process, ilmenite is limited as a feed. The Austpac process is less effective because it requires higher acidity for the leaching of the remaining magnetic iron. The Dunn process is also considered less environmentally friendly because of the highly corrosive Cl_2 handling process, while the Kataoka, Altair, and BHP Billiton processes are also considered less environmentally friendly because of the subsequent leaching process ([Nguyen and Lee, 2019](#)). The Becher process involves reducing the iron in ilmenite to metallic iron by way of burning coal at 1200°C followed by aeration and leaching to remove the metallic iron ([Gázquez et al., 2014](#)).

*Corresponding author's email: sri.harjanto@ui.ac.id, Tel.: +62-21-7863510; Fax.: +62-21-7872350
doi: [10.14716/ijtech.v12i6.5232](https://doi.org/10.14716/ijtech.v12i6.5232)

Many aspects of the carbothermic reduction process of ilmenite have attracted much research. [Tripathy et al. \(2012\)](#) reduced ilmenite at 1000–1150°C using graphite and coke as reducing agents. According to the findings, graphite is effective as a reducing agent at a reduction temperature of 1150°C, and it can work within a shorter time interval. Meanwhile, coke is more effective when heated to 1000°C. [El-Hussiny et al. \(2008\)](#) reduced ilmenite with breeze coke at 800–1200°C and discovered that reducibility increased with the stoichiometric amount of coke. Furthermore, the rate of reduction increased as the temperature rose. [Bhalla et al. \(2017\)](#) carried out the carbothermic reduction of ilmenite with graphite as the reducing agent at temperatures between 1050°C and 1350°C under an argon atmosphere. They reported that the rate of reduction increased with increases in temperature and decreases in particle size. Ilmenite reduction can be accomplished through a step in which iron oxide is first reduced to metallic iron and then to iron carbide, while titanium oxide is initially reduced to Ti_nO_{2n-1} with the possibility of later lower oxide formation. The particle core (original ilmenite grain) retains its composition, with a slight reduction in iron and titanium oxides in the early stages of reduction and is partially reduced in later stages. According to [Wang et al. \(2008\)](#), the reduced ilmenite phase formed by graphite contains iron, ilmenite, rutile, reduced rutile, pseudorutile, and graphite below 1200°C. From 900–1000°C, however, reduced rutile was absent. Above 1200°C, the Ti_3O_5 phase appears alongside iron, rutile, reduced rutile, Fe_3C , and pseudobrookite solid solution.

The utilization of biomass as an alternative carbon source has been studied in many fields, for example, the co-gasification process with blending fuel (biomass and coal) and reductant agents in the carbothermic reduction of minerals. [Ahmad et al. \(2020\)](#) investigated the effect of a torrefied palm kernel shell and Mukah Balingian coal on product yield and gaseous composition in the co-gasification process. They concluded that pretreatment with this biomass mixture resulted in higher gas yields and lower tar and charcoal yields, thereby improving the co-gasification performance. Meanwhile, many researchers have investigated the use of biomass (including palm oil waste) as a renewable carbon source for the carbothermic reduction process of minerals and ores. Using the biomass of palm kernel shell waste as a reducing agent, iron oxide in low-grade iron ore could be reduced completely to magnetite and partially to wustite when up to 30% of the biomass was used in the reduction process ([Abd Rashid et al., 2014](#)). Adding up to 30% of sawdust biomass containing 12.5% fixed carbon and 80.7% volatile matter successfully reduced the iron ore to its metallic iron phase at 1200°C ([Strezov et al., 2006](#)). Furthermore, [Srivastava et al. \(2013\)](#) investigated the use of fine wood biomass as a reducing agent in the smelting of magnetite concentrate. They found that pig iron nuggets with metallization of 98.10% and a total Fe of 97.16% could be produced at a temperature of 1450°C and a reaction time of 20 min. In addition, [Zhang et al. \(2017\)](#) studied the roasting process of low-grade limonite ore with biomass at temperatures of up to 750°C for 45 min in a vacuum atmosphere. They reported that after dehydration at high temperatures, the iron-bearing materials in limonite ore became $\alpha-Fe_2O_3$, which was then reduced to Fe_3O_4 by biomass reduction. Fe_3O_4 will convert to Fe_2SiO_4 at temperatures above 650°C, causing magnetic materials to be reduced and the calcined ore's magnetism to be weakened. Furthermore, at a temperature of 550°C with a biomass ratio of 15%, the recovery rate and iron grade were 72% and 58%, respectively.

However, published reports on the use of biomass as a reducing agent in the upgrading process of ilmenite are still lacking. [Ismail et al. \(1982\)](#) investigated the decomposition of preoxidized ilmenite using sawdust biomass as a reducing agent at 1100°C for 3 h. They reported that two steps occurred during the decomposition process. The first step was the

conversion of Fe^{3+} in ferric pseudobrookite to Fe^{2+} in ilmenite. At this point, the concentration of ferric pseudobrookite decreased over time, while the concentration of ilmenite increased. This indicates that ilmenite was reformed by a recombination reduction mechanism in the early stages of reduction. The second step was the conversion of Fe^{2+} to metallic iron. As a result, the concentration of ilmenite gradually decreased, while the concentrations of metallic iron and rutile increased (suboxides of titanium). Recently, [Setiawan et al. \(2020\)](#) investigated the carbothermic reduction of ilmenite using palm kernel shells as a reducing agent. They found that a reduction temperature of 1200°C using a solar furnace promoted pseudobrookite formation, and a unique line morphology in metallic iron was observed instead of the spherical structure found in samples heated in electric furnaces. They found that the mechanisms behind the carbothermic reduction of complex weathered ilmenite using the biomass of palm kernel shells and graphite as reducing agents were based on the diffusion of oxygen atoms ([Setiawan et al., 2021](#)).

Thus, this research aims to investigate the effects of biomass addition during the carbothermic reduction of ilmenite on phase transformation and microstructure evolution. The phase characterization and detailed microstructures during the carbothermic reduction of ilmenite at up to 1200°C for different reaction times were observed and discussed.

2. Materials and Methods

2.1. Materials Description and Characterisation

The ilmenite ore used in the current study was supplied by PT Monokem Surya, Karawang, West Java Province, Indonesia. Ilmenite's particle size distribution analysis was carried out using a particle size analyzer (PSA, Cilas 1190) in wet mode. Furthermore, the chemical compositions of ilmenite ore were examined using X-ray fluorescence (XRF; Philips PW2404). Detailed characterization using XRF has been described elsewhere ([Setiawan et al., 2020](#)).

2.2. Preparation and Analysis of Biomass

The reducing agent used in this study was biomass derived from palm kernel shells obtained from local industrial waste. First, the palm kernel shell waste was cleaned and dried at a temperature of 100°C for 1 h in the oven to remove moisture. Subsequently, the palm kernel shell waste was reheated in the oven for 1 h at a temperature of 300°C and then reheated in a furnace at a temperature of 750°C for 3 h. After heating, the biomass was reduced using a pulverizer machine for 4 min to obtain a finer particle size. The particle size distribution of the biomass was also characterized using the wet method (Cilas 1190).

The proximate analysis of the biomass to calculate the fixed carbon, moisture in air-dried, ash, and volatile matter was measured according to ASTM D.3172, D.3173, D.3174, and D.3175, respectively. For the ultimate analysis of the biomass, carbon, hydrogen, and nitrogen were determined according to ASTM D.5373, and total sulfur and oxygen were calculated according to ASTM D.4239 and D.3176, respectively.

2.3. Carbothermic Reduction Experiment

Ilmenite, biomass, organic binder (carboxymethyl cellulose), and distilled water had mixed homogeneity. The addition levels of biomass were set to 6, 8, 9, and 10 wt.%. Furthermore, the mixture was compressed into a pellet sample with a diameter of 20 mm and a height of 10 mm. Then, the pellet sample was dried at 100°C for 5 h.

The reduction process experiments in the current study were conducted in a horizontal tube furnace (GSL-1700X). The pellet samples were placed in the alumina crucible boat and put into the hot zone of the tube furnace. Argon gas flowed (0.6 L/min) into the alumina

tube to maintain an inert atmosphere. The samples were reduced at 1000°C, 1100°C, and 1200°C for different reaction times (0.5, 1, 2, and 3 h).

2.4. Phase and Microstructure Characterisation

The reduced samples (powder samples) were examined by X-ray diffraction (XRD; Rigaku MiniFlex II) with a Cu K α source ($\lambda=1.54178$ Å) to identify phase compositions. XRD was operated at 15 mA and 30 kV at a scanning rate from 10°–90° (2 θ) with a scan speed of 4° per min. Phase identification was analyzed using HighScore Plus software with the ICSD database, and a semi-quantitative phase analysis was carried out using the Rietveld method. The Scherrer equation was used to calculate the crystallite size (Suryanarayana et al., 1998). The relationship between crystallite size values is inversely proportional to the full width at half maximum (FWHM) value, as shown in the equation below:

$$D = \frac{k\lambda}{\beta \cos\theta} \quad (1)$$

where D is the size of the crystallites (nm), k is the Scherrer constant (0.9), λ is the wavelength of the X-ray sources (0.15406 nm), β is the FWHM value (radians), and θ is the peak position (radians).

The reduced samples were mounted in epoxy resin and then polished with up to 1200-grit silicon carbide paper before microstructure analysis using an optical microscope (OM; Zeiss Primotech). The OM images were used as input data to measure the average particle size of metallic iron using the free software ImageJ (version: 1.52o, Java 1.8.0_112). The metallic iron size of the microstructure image was measured by selecting the metallic iron area with polygon selection in ImageJ software. Measurement repetition was undertaken to ensure the reproducibility of the data.

3. Results and Discussion

3.1. Raw Material Characteristics

The mean diameter of the ilmenite ore concentrate particles was 231 μm , with D_{80} of 300 μm . The particle size distribution of the ilmenite ore concentrate is shown in Figure S1 (a). The chemical composition of the ilmenite sample is listed in Table S1. The results indicated that the sample contained a high amount of titanium and iron at 50.2 wt.% TiO₂ and 37.05 wt.% Fe₂O₃, respectively. Major impurities in the concentrate include Cr₂O₃ (4.245 wt.%), Al₂O₃ (2.06 wt.%), MgO (1.54 wt.%), Mn₃O₄ (1.505 wt.%), SiO₂ (0.39 wt.%), ZrO₂ (0.245 wt.%), P₂O₅ (0.16 wt.%), Nb₂O₅ (0.157 wt.%), and V₂O₅ (0.231 wt.%). The mineralogy, phase, microstructure, and elemental mapping of the ilmenite concentrates have been discussed comprehensively in a previous study (Setiawan et al., 2020; Setiawan et al., 2021).

The mean diameter and D_{80} of the pulverized biomass from the palm kernel shell were 14.5 μm and 23.31 μm , respectively. The particle size distribution is shown in Figure S1 (b). The size distribution of the biomass was finer than that of the ilmenite ore concentrate. Furthermore, the calorific value, proximate, and ultimate analysis of palm kernel shell biomass are presented in Table S2. The analysis of pulverized biomass revealed that the biomass contained a high amount of fixed carbon at 79 wt.%. It also contained a high amount of volatile matter and moisture, as much as 11 wt.% and 6 wt.%, respectively.

3.2. Phase Transformation and Phase Stability during Reduction

Figure 1 shows the XRD patterns of the samples. Several phases, such as ilmenite (FeTiO₃), pseudobrookite (FeTi₂O₅), metallic iron (Fe), rutile (TiO₂), and spinel (MgAl₂O₄), were observed in all the reduced samples. The peak intensity of metallic iron and rutile increased with increasing temperature, while the peak intensity of ilmenite and spinel

decreased. At 1200°C, the ilmenite and spinel phases were no longer present, and anosovite (Ti_3O_5) was formed instead. TiO_2 is a stable oxide with resistance to high temperatures, and as a result, TiO_2 remained unaffected under reaction conditions, while FeO was reduced to metallic iron (Sarkar et al., 2016).

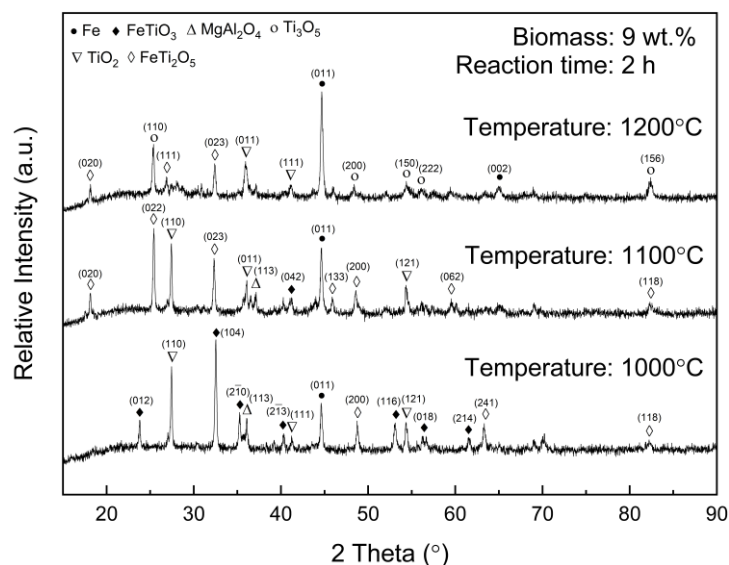


Figure 1 XRD patterns showing the phases formed after reduction at different temperatures

As shown in Figure 2a, the addition of 6 wt.% biomass in the carbothermic reduction process produced ilmenite (FeTiO_3), pseudobrookite (FeTi_2O_5), metallic iron, rutile (TiO_2), and spinel (MgAl_2O_4) phases. The peak intensity of metallic iron increased with the addition of 8–9 wt.%, followed by a decrease in pseudobrookite and the disappearance of peaks in the ilmenite and spinel phases. Following the addition of 10 wt.%, the appearance of the anosovite (Ti_3O_5) phase as a result of carbothermic reduction by carbon contained in the reducing agent in the following steps was observed: ilmenite \rightarrow pseudobrookite \rightarrow metallic iron, and Ti oxide (rutile and anosovite).

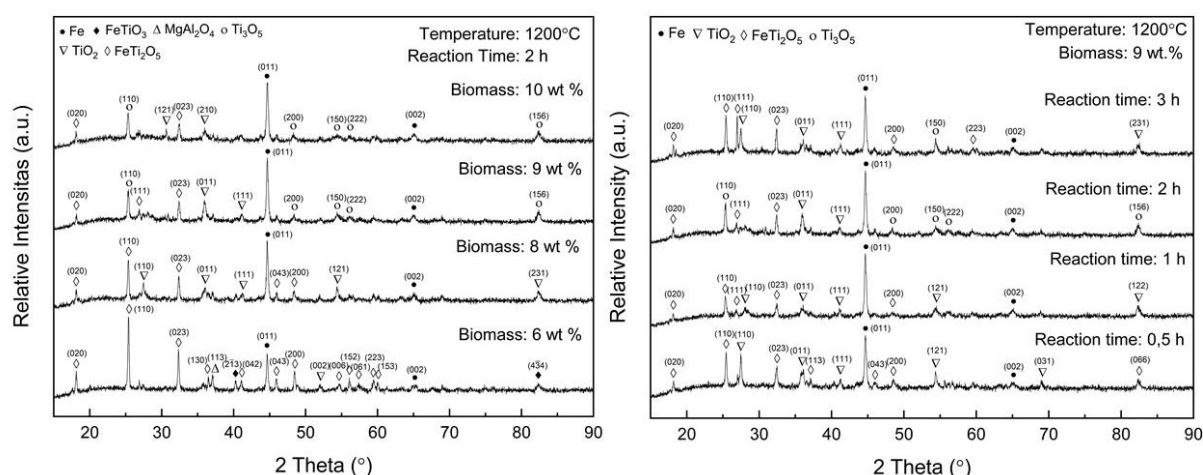


Figure 2 Phase formation after reduction at: (a) varying amounts of palm kernel shell biomass; and (b) different reaction times at 1200°C and biomass addition of 9 wt.%

However, the effect of reaction time on phase transformation was investigated (Figure 2b). The phases formed during the 0.5 h reaction time were pseudobrookite, rutile, and metallic iron. The peak intensity of pseudobrookite decreased after 1 to 2 h of reaction time

due to the reduction of pseudobrookite to rutile and metallic iron, as indicated by the increasing peak intensity of the two phases. The peak intensity of metallic iron decreased after 3 h of reaction time.

The reaction of pseudobrookite was reduced to rutile and metallic iron:



Based on the binary diagram (log $p\text{O}_2$ with composition) constructed using the FactSage 7.2 thermochemical package in Figure 3a, the more reductive the carbothermic reaction is at a reduction temperature of 1200°C, the more the Fe_2O_3 +rutile phase will transform into rutile + spinel and then into pseudobrookite + spinel. Then, they transform into ilmenite + spinel, and so on. Finally, in the most reductive condition, the formed phase is $\text{Fe}_{\text{FCC}} + \text{Ti}_{20}\text{O}_{39}$. This confirmed the XRD semi-quantitative data in Figure 3b that the concentration of the phases formed by the addition of 9 wt.% at a reduction temperature of 1200°C for 2 h was 8.9% metallic iron, 50.3% Ti_3O_5 , 23.6% rutile, and 17.3% pseudobrookite.

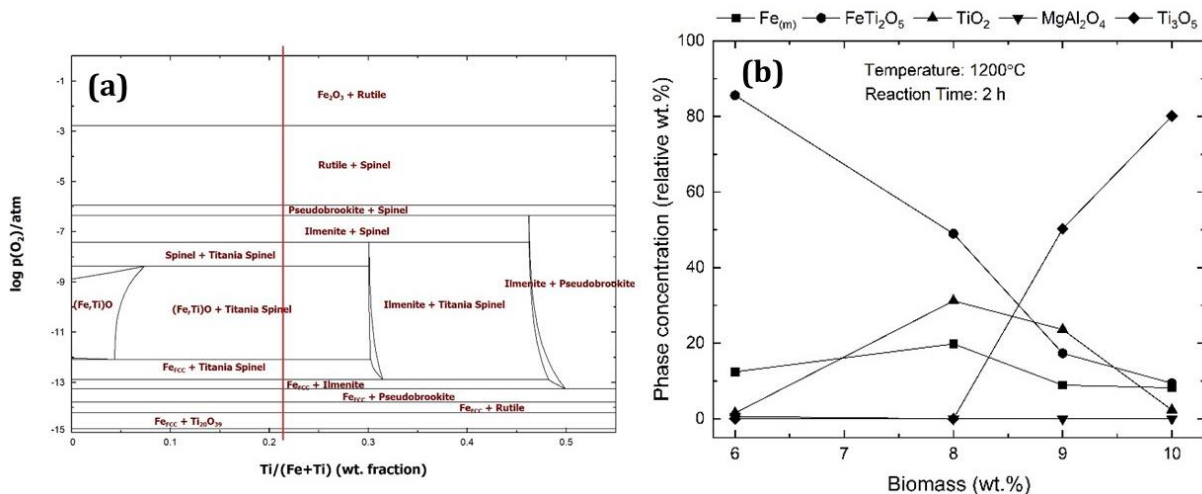


Figure 3 (a) Fe-Ti-O₂ binary diagram at 1200°C. The line shows the conditions of the present study; (b) Phase concentration of the product measured by semi-quantitative XRD

3.3. Crystallite Size

Figure 2 shows that the peaks of metallic iron and rutile changed due to variations in temperature and biomass addition. The calculation of the crystallite sizes of the reduced samples showed that the average crystallite sizes of metallic iron and rutile at a temperature of 1200°C for 2 h with a 9 wt.% biomass addition were 24.13 and 21.68 nm, respectively.

Figure 4 shows the average crystallite size, which was affected by: (a) the temperature at the addition of 9 wt.% of biomass for 2 h; and (b) the biomass addition reacted at 1200°C for 2 h. Figure 4a reveals that the average crystallite size decreased as the temperature increased for metallic iron and rutile. The crystallite size of metallic iron was larger than that of rutile. However, with the addition of biomass less than 7 wt.%, the crystallite size of rutile was higher than metallic iron. This indicated that, compared to rutile, the crystal growth of metallic iron was hindered during the carbothermic reduction of ilmenite with a biomass addition of less than 7 wt.% at 1200°C for 2 h. The addition of biomass of more than 8 wt.% increased the crystallite size of metallic iron and rutile (see Figure 4b). Additionally, it was observed that the average crystallite size of metallic iron was higher than that of rutile.

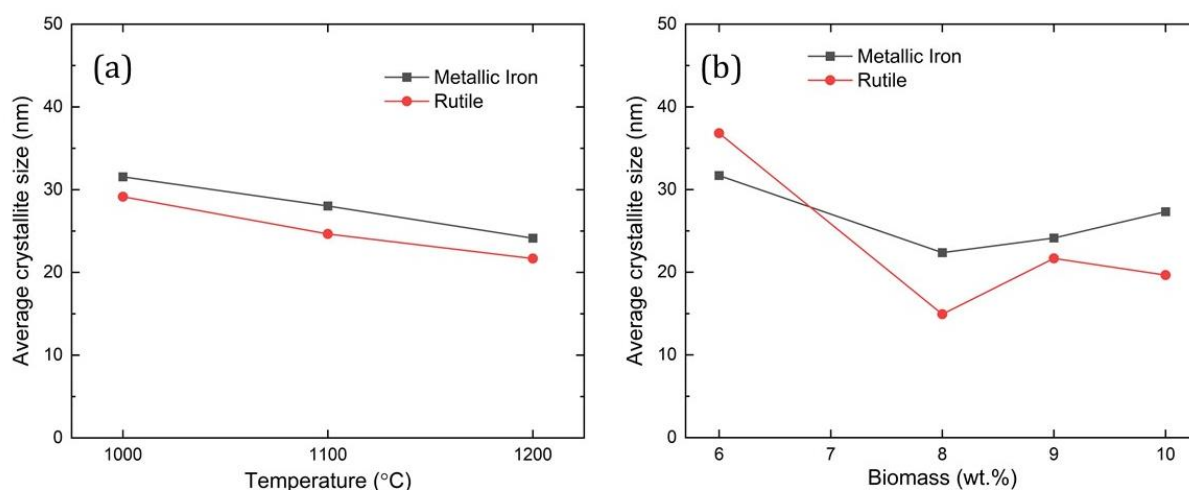


Figure 4 Crystallite size of metallic iron and rutile as affected by (a) temperature with the 9 wt.% addition of biomass and (b) biomass addition at 1200°C

3.4. Microstructures and Grain Morphologies

Typical microstructures of the reduced samples consisted of bright metallic iron and gray slag phases (see Figure S2). The sample particle's porosity was also observed due to gas evolution during the carbothermic reaction or weathering process. The morphology of metallic iron followed the shape of porosity previously formed during the weathering process. An increase in reaction temperatures resulted in a more granular morphology of metallic iron in the sample particles. At higher temperatures, for instance, at 1200°C, many pores were formed due to gas evolution, thus promoting the permeability of the particles for the reduction reaction and resulting in the formation of a large amount of metallic iron. In general, metallic iron grains grow because of nucleation and aggregation, and they continue to grow as the temperature of the environment increases (Run et al., 2019).

Figure 5 depicts the microstructures of the samples reduced at 1200°C for 2 h with the variation in the added biomass. The greater the amount of biomass added, the larger the area covered by metallic iron grains. The shape of metallic iron grains consisted of streaks and granules. Qualitatively, the granule form of metallic iron in the sample particle spread with a higher amount of added biomass.

The morphology of metallic iron grains also consisted of a streak and granule form due to variations in holding time during the reduction reaction (Figure S3). Figure S3 also shows that the longer the reaction time, the larger the metallic iron formed because of grain growth and aggregation in its vicinity.

3.5. Metallic Iron Grain Size

The effects of the biomass addition on the average size of metallic iron formed after the reduction process at varying temperatures and reaction times are depicted in Figures 6a and 6b, respectively. The addition of more biomass at certain temperatures increased the average grain size of metallic iron (Figure 6a). It can be observed that the addition of 9 wt.% biomass resulted in the largest average grain size of metallic ore. Similarly, by varying the reaction time for each different amount of biomass added, the largest average grain size of metallic iron formed resulted from the addition of 9 wt.% biomass. The reaction time of 2 h resulted in the largest average grain size of metallic iron in the range of added biomass (see Figure 6b).

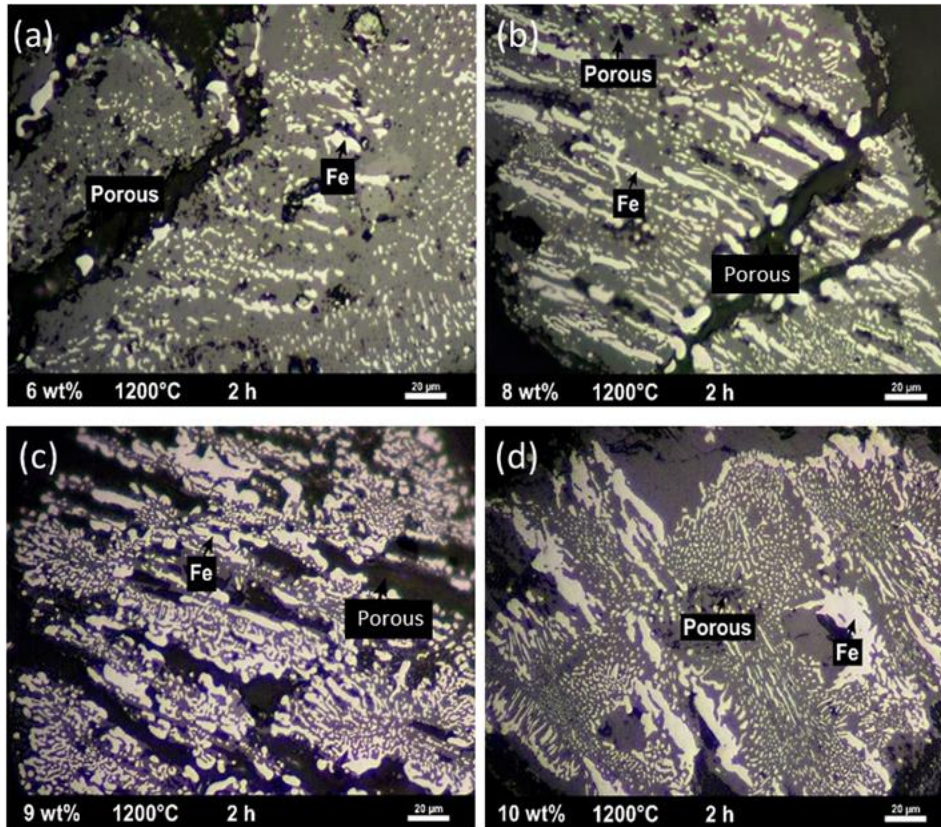


Figure 5 Microstructures of the reduced samples reacted at 1200°C for 2 h with various amounts of added biomass of: (a) 6 wt.%; (b) 8 wt.%; (c) 9 wt.%; and (d) 10 wt.%

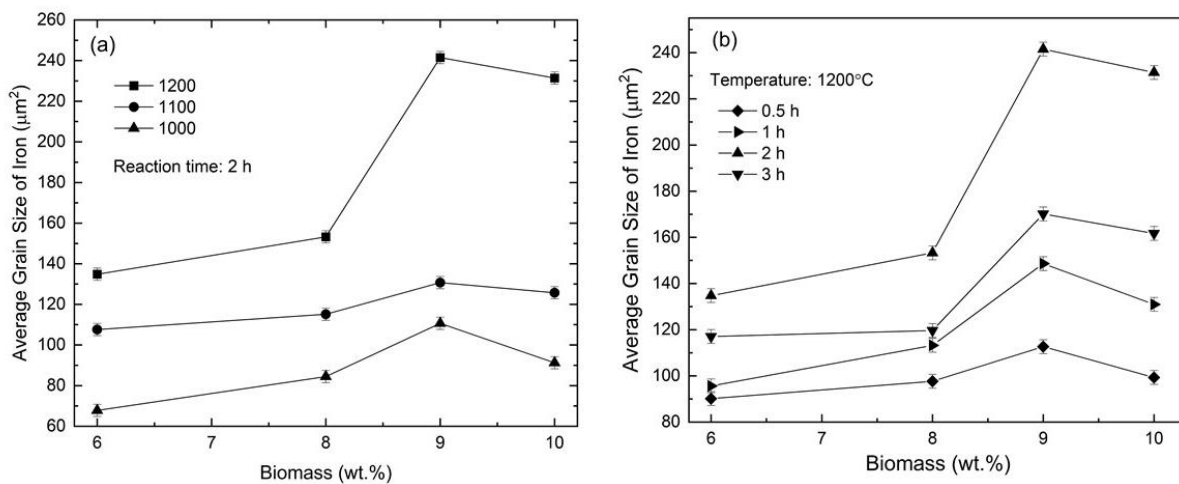


Figure 6 (a) The influence of biomass addition and temperature on the average grain size of metallic iron formed during the reduction process; and (b) the influence of biomass addition and reaction time on the average grain size of metallic iron formed during the reduction process

A comparison of the crystallite (Figure 4a) and grain sizes of metallic iron data (Figure 6a) showed that the crystallite size decreased with increasing reaction temperatures, whereas the average grain size increased with increasing temperatures. At this stage, the relationship between the crystallite size and the average grain size of metallic iron is still unclear. It seems that the grain growth of metallic iron is promoted by the accumulation of relatively small crystals, not by the increase in crystallite size.

4. Conclusions

The effects of adding palm kernel shell biomass as a reducing agent on the carbothermic reduction of ilmenite were studied. The following conclusions were drawn: (1) The phase analysis showed the near-complete dissociation of ilmenite at 1200°C for 2 h with the addition of 6 and 8 wt.% biomass. Complete dissociation was reached as more biomass was added. At this point, the phases formed were metallic iron, rutile, pseudobrookite, and anosovite; (2) The morphology of metallic iron consisted of the streak and granule shapes. The particle size of metallic iron was greatly enhanced with increased added biomass. The maximum average grain size of metallic iron formed was found to be 241.5 μm^2 with the addition of 9 wt.% of biomass at 1200°C for 2 h.

Acknowledgements

The authors would like to express their gratitude for the financial support from the Directorate of Research and Public Engagement, Universitas Indonesia, under the PUTI Prosiding Grant 2020 (NKB-1199/UN2.RST/HKP.05.00/2020) and the PUTI Kolaborasi Internasional 2020 (NKB-797/UN2.RST/HKP.05.00/2020). PT Monokem Surya, Karawang, Indonesia is thanked for providing ilmenite concentrate. Dr. Mark I Pownceby (CSIRO Mineral Resources, Australia) is gratefully acknowledged for providing XRF data.

References

- Ahmad, R., Ishak, M.A.M., Ismail, K., Kasim, N.N., Mohamed, A., Ani, A., Radzun, K., 2020. The Effect of Pretreated Palm Kernel Shell and Mukah Balingian Coal Co-Gasification on Product Yield and Gaseous Composition. *International Journal of Technology*, Volume 11(3), pp. 501–510
- Abd Rashid, R.Z., Salleh, H.M., Ani, M.H., Yunus, N.A., Akiyama, T., Purwanto, H., 2014. Reduction of Low Grade Iron Ore Pellet using Palm Kernel Shell. *Renewable Energy*, Volume 63, pp. 617–623
- Bhalla, A., Kucukkargoz, C.S., Eric, R.H., 2017. Solid-State Reduction of an Ilmenite Concentrate with Carbon. *Journal of the Southern African Institute of Mining and Metallurgy*, Volume 117(5), pp. 415–421
- El-Hussiny, N.A., Lasheen, T.A., Shalabi, M.E.H., 2008. Kinetic Reduction of Rosetta Ilmenite with Coke Breeze and Beneficiation of the Product. *The Journal of Ore Dressing*, Volume 9(18), pp. 8–16
- Gázquez, M.J., Bolívar, J.P., García-Tenorio García-Balmaseda, R., Vaca, F., 2014. A Review of the Production Cycle of Titanium Dioxide Pigment. *Materials Sciences and Applications*, Volume 5(7), pp. 441–458
- Ismail, M.G.M.U., Amarasekera, J., Kumarasinghe, J.S.N., 1982. Studies on Decomposition of Ilmenite from Sri Lanka. *Journal of the National Science Foundation of Sri Lanka*, Volume 10(1), pp. 107–127.
- Nguyen, T.H., Lee, M.S., 2019. A Review on the Recovery of Titanium Dioxide from Ilmenite Ores by Direct Leaching Technologies. *Mineral Processing and Extractive Metallurgy Review*, Volume 40(4), pp. 231–247
- Run, H., Xiaodong, L., Qinghui, W., Qinzhi, W., Jinzhu, Z., 2019. Non-Isothermal Reduction Kinetics of Iron During Vacuum Carbothermal Reduction of Ilmenite Concentrate. *Metallurgical and Materials Transactions B*, Volume 50(2), pp. 816–824
- Sarkar, B.K., Samanta, S., Dey, R., Das, G.C., 2016. A Study on Reduction Kinetics of Titaniferous Magnetite Ore Using Lean Grade Coal. *International Journal of Mineral Processing*, Volume 152, pp. 36–45

- Setiawan, A., Rhamdhani, M.A., Pownceby, M.I., Webster, N.A.S., Harjanto, S., 2021. Kinetics and Mechanisms of Carbothermic Reduction of Weathered Ilmenite using Palm Kernel Shell Biomass. *Journal of Sustainable Metallurgy*, pp. 1-19
- Setiawan, A., Shaw, M., Torpy, A., Pownceby, M.I., Harjanto, S., Rhamdhani, M.A., 2020. Solar Carbothermic Reduction of Ilmenite using Palm Kernel Shell Biomass. *The Journal of the Mineral*, Volume 72(10), pp. 3410–3421
- Srivastava, U., Kawatra, S.K., Eisele, T.C., 2013. Production of Pig Iron by Utilizing Biomass as a Reducing Agent. *International Journal of Mineral Processing*, Volume 119, pp. 51–57
- Strezov, V., 2006. Iron Ore Reduction using Sawdust: Experimental Analysis and Kinetic Modelling. *Renewable Energy*, Volume 31(12), pp. 1892–1905
- Suryanarayana, C., Norton, M.G., 1998. *X-Ray Diffraction a Practical Approach*. New York: Springer Science+Business Media New York, pp. 207–221
- Tripathy, M., Ranganathan, S., Mehrotra, S.P., 2012. Investigations on Reduction of Ilmenite Ore with Different Sources of Carbon. *Mineral Processing and Extractive Metallurgy*, Volume 121(3), pp. 147–155
- U.S. Geological Survey., 2021. Mineral commodity summaries 2021: U.S. Geological Survey, p. 200.
- Wang, Y.M., Yuan, Z.F., Guo, Z.C., Tan, Q.Q., Li, Z.Y., Jiang, W.Z., 2008. Reduction Mechanism of Natural Ilmenite with Graphite. *Transactions of Nonferrous Metals Society of China*, Volume 18(4), pp. 962–968
- Zhang, K., Chen, X.L., Guo, W.C., Luo, H.J., Gong, Z.J., Li, B.W., Wu, W.F., 2017. Effects of Biomass Reducing Agent on Magnetic Properties and Phase Transformation of Baotou Low-Grade Limonite During Magnetizing-Roasting. *PLOS one*, Volume 12(10), pp. 1–18